Sound radiation and transonic boundaries of a plate with an acoustic black hole

Li Ma and Li Cheng[a)]
Department of Mechanical Engineering, The Hong Kong Polytechnic University, Hung Hom, Kowloon, Hong Kong, People's Republic of China

(Received 31 July 2018; revised 7 November 2018; accepted 10 November 2018; published online 9 January 2019)

The acoustic black hole (ABH) phenomenon has shown promise for noise and vibration control applications. In this paper, a two-dimensional (2-D) Daubechies wavelet (DW) model is established for the sound radiation prediction of plates embedded with a circular ABH indentation. ABH plates are shown to exhibit a reduced sound radiation efficiency as compared with their flat counterpart. Below the critical frequency, this is caused by the weakening of the structural stiffness due to the ABH indentation. Above the critical frequency, a subsonic region inside the ABH cell may appear, containing acoustically slow structural waves. This region, confined within a transonic boundary, is due to the ABH-specific phase velocity reduction of the bending waves. Drawing energy away from the supersonic region of the plate, this subsonic region warrants a reduced sound radiation to the far field. Numerical results on the investigated configuration show an increase in the sound radiation efficiency due to the added stiffness effect of damping layers. Sound radiation efficiency alongside the transonic boundary changes is scrutinized and quantified. Visualization of the supersonic acoustic intensity and radiation allows identifying the effective sound radiation regions of ABH plates and their relationship with the transonic boundaries at different frequencies.
 https://doi.org/10.1121/1.5081680

[NX] Pages: 164–172

I. INTRODUCTION

Lightweight structures with high damping and low sound radiation capability are in great demand for various applications in aerospace, automobile, and marine industries. Among possible options to increase the structural damping, viscoelastic coating is probably the most popular one for attenuating flexural vibrations and reducing their sound radiation.[1] In conventional structures, however, vibration energy, due to its dispersive nature, usually spreads over the entire structure. Therefore, a damping treatment needs to be applied over a large portion of the structure in order to bring the overall system damping up to an appreciable level,[2] thus resulting in an overall increase in the structure weight. Recently, the concept of an "acoustic black hole (ABH)"[3,4] has been explored as a passive and lightweight approach which shows promise in controlling bending vibrations and reducing sound radiation of structures.

The ABH phenomenon results from the flexural wave propagation inside a thin-walled structure with a tailored power-law thickness profile. Taking the one-dimensional (1-D) case as an example, an ABH beam features a smooth decrease in its local thickness according to $h(x) = \varepsilon x^{\gamma}$ $(\gamma \geq 2)$ along its longitudinal direction x. The gradually decreased thickness allows for the slowing-down of the phase and group velocity of the bending waves, theoretically to zero, alongside a dramatically amplified vibration amplitude. For real structures with an inevitable truncated edge, the use of a small amount of damping material over the tip area of the taper is shown to enable a significant energy localization and dissipation.[5] Owing to this unique feature, various ABH structures, mostly beams[6–8] and plates,[9] have been investigated in an accelerating pace in the literature, both numerically[10,11] and experimentally.[12] Non-ideal ABH structures containing geometrical imperfections or different thickness profiles have also been investigated.[13,14]

As compared with the work on vibration control or its utilization for energy harvesting,[15,16] studies on sound properties of the ABH structures are much less. Using a finite element/boundary element (FE/BE) model, the sound radiation of plates with embedded periodic ABHs was investigated by Conlon *et al.*[17] Results showed that a panel with periodic ABH cells can substantially reduce the radiated sound power, compared with a uniform panel. Using a wavenumber transform analysis,[18] Feurtado and Conlon demonstrated that ABHs redistribute the supersonic vibration into subsonic components and act as structural acoustic decouplers, resulting in a reduction in the sound radiation efficiency. Bowyer and Krylov[19] experimentally measured the radiated sound power of a plate with multiple ABH indentations containing a physical hole at the center. As a result, the observed reduction in the sound radiation is the combined ABH result with that of the acoustic short circuiting due to the hole. Apart from the sound radiation problem, sound transmission of ABH plates was also experimentally and numerically investigated.[20] The observed phenomena are consistent with and can be explained by the basic structural acoustic principle.

Most existing works mainly rely on finite-element method/boundary-element method (FEM/BEM) simulations and experiments, with inherent advantages in handling

[a)]Electronic mail: li.cheng@polyu.edu.hk

complex structures. In this paper, we attempt to propose a two-dimensional (2-D) semi-analytical ABH model as an alternative to FEM/BEM, on which some fundamental ABH-specific sound radiation issues are revisited. As illustrated in our previous work,[21] the modelling of the ABH structures is technically challenging due to their ABH-specific features. On one hand, an ABH structure features a strong wavelength variation over the structure. On the other hand, ABH effects are most prominent above the cut-on frequency[17] or characteristic frequency,[21] when the structural wavelength starts to be comparable with the characteristic dimension of the ABH cells. Therefore, an ideal simulation method should be endowed with the dual capability of accommodating the space-varying character of the wavelength and reaching the high frequency range at the same time. On top of this, there is the need of considering the full coupling between the structure and the add-on damping treatment,[21] since in the thinnest part of the ABH cells, the mechanical properties of the coating and its coupling with the base structure may become non-negligible.

Motivated by this, the main objective of the present work is to investigate and scrutinize the sound radiation properties of a plate with an embedded circular ABH indentation by revamping a previously developed semi-analytical 2-D wavelet vibration model.[21] Particular attention is paid to the description and understanding of the underlying physical process of the sound radiation in different frequency ranges, with the help of relevant physical parameters such as changes of the transonic boundaries inside the ABH indentation and supersonic acoustic intensity.[22,23] Results are expected to enrich the existing understanding on the sound radiation of ABH structures.

The rest of the paper is organized as follows. The proposed 2-D Daubechies wavelet (DW) acoustic model is presented in Sec. II, in which both the far-field and near-field methods are adopted. Calculation of the supersonic acoustic intensity of the radiated sound in spatial domain is also formulated. In Sec. III, investigations into the sound radiation of ABH plates are performed through examining the radiated sound power and sound radiation efficiency of the ABH plate in different frequency ranges. The observed reduction in the sound radiation is scrutinized and quantified by examining the ABH-induced structural stiffness changes in the low frequency range and the creation and evolution of the transonic boundary in the high frequency range. Supersonic acoustic intensity in spatial domain is then exploited to identify the vibrating regions that are responsible for the effective sound radiation to the far field. Effect of the damping layers on sound radiation efficiency is also investigated, showing the non-negligible added stiffness effect for the investigated configuration. Finally, conclusions are drawn.

The present work attempts to claim a three-fold novelty: (1) A wavelet-based model is established for the acoustic radiation prediction as an alternative to the FEM/BEM. (2) ABH effect on the sound radiation is demonstrated and physically explained using parameters such as supersonic acoustic intensity and transonic boundary changes. This allows the visualization of the sound radiation in spatial domain and hopefully enriches the existing understanding on the sound radiation of ABH structures. (3) The stiffness effect of damping layers on the increase of the sound radiation efficiency calls for a careful handling of the viscoelastic coating for sound radiation applications.

II. THEORY

A. Summary of the 2-D semi-analytical vibration model

For the completeness of the paper, a previously developed ABH plate model[21] is briefly recalled. We consider a rectangular plate shown in Fig. 1. The plate (with a lateral dimension of a, b) contains a circular ABH indentation, with each side symmetrically coated with a damping layer of uniform thickness h_d. The circular indentation has a radius of R_{ABH}, centered at (x_c, y_c). The thickness of the uniform part of the plate is h, while that of the circular ABH indentation changes according to $h(x,y) = \varepsilon(\sqrt{(x-x_c)^2 + (y-y_c)^2})^{\gamma} + h_0$, where ε is a constant, γ the power law index, and h_0 the smallest thickness of the indentation. The central portion of the ABH indentation within a radius R_d is covered with the damping layer. Various types of boundary conditions can be achieved using a set of artificial springs, uniformly distributed along the edges of the plate.[24] A complex Young's modulus which includes material loss is introduced to different constituents of the plate assembly: $E_0^* = E_0(1 + i\eta_0)$ and $E_d^* = E_d(1 + i\eta_d)$ for the plate and damping layers, respectively, in which η_0 and η_d are the corresponding loss factors. The damping layer is explicitly modeled as an integrate part of the ABH plate, with both its stiffness and mass included in the global matrices of stiffness and mass of the whole system.[21] Although there exist more complex and general distributed loads,[20] we only consider the case of a point force excitation $f(t)$ in this paper.

The system is assumed to be symmetrical with respect to its mid-plane, in which case, Love–Kirchhoff thin plate theory can be applied to describe its displacement field as

$$\{u, v, w\} = \left\{-z\frac{\partial w}{\partial x}, -z\frac{\partial w}{\partial y}, w\right\}, \tag{1}$$

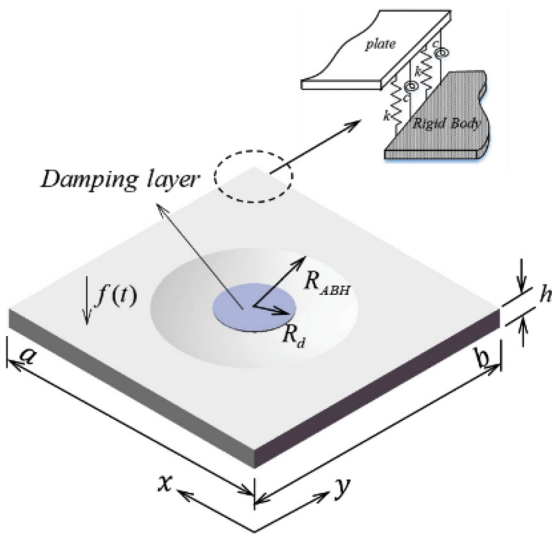

FIG. 1. (Color online) Modelling of the ABH plate.

where vector $\{u, v, w\}$ contains the three displacements of a point, in either the plate or the damping layers.

Under Rayleigh–Ritz framework, w is decomposed over a set of assumed admissible functions. In the dimensionless coordinates $\xi = x/a$ and $\eta = y/b$, w can be expressed as

$$w = \sum_{i=1}^{p}\sum_{j=1}^{q} a_{ij}(t)\varphi_i(\xi)\varphi_j(\eta), \tag{2}$$

in which $\varphi_i(\xi)$ and $\varphi_j(\eta)$ are the admissible functions; p and q are the numbers of terms to be kept in the computation. Complex coefficients $a_{ij}(t)$ are to be determined. p and q should be carefully selected to ensure the convergence of the calculation.[21] Following the conventional Hamilton principle and applying Euler–Lagrange equations, we can get the equation of motion of the system, cast into a matrix form as

$$\boldsymbol{M}\ddot{\boldsymbol{a}}(t) + \boldsymbol{K}\boldsymbol{a}(t) = \boldsymbol{f}(t), \tag{3}$$

where $\boldsymbol{M}$ and $\boldsymbol{K}$ represent the global mass and stiffness matrices, respectively; $\boldsymbol{f}(t)$ is the excitation force vector.

B. Sound radiation model

The sound radiation of the ABH plate is characterized using three metrics: radiated sound power, sound radiation efficiency and supersonic acoustic intensity. The supersonic acoustic intensity is useful to identify the region of ABH plates that effectively radiates sound into the far field. The aforementioned vibration model is extended to accommodate this need under the wavelet-based framework.

1. Sound power and sound radiation efficiency

The acoustic model used in the analyses is shown in Fig. 2. The plate is assumed to be bounded by an infinitely large and rigid baffle. Setting the origin of the coordinates at the center of the plate, with x-y plane coinciding with the mid-plane of the plate, Rayleigh integral[25] can be used to calculate the sound pressure radiated into the far field in an infinitely large half space as

$$\boldsymbol{p}(r) = \frac{j\omega\rho_a}{2\pi}\int\int_S \boldsymbol{v}(r_0)\frac{\exp(-jk|r-r_0|)}{|r-r_0|}dS, \tag{4}$$

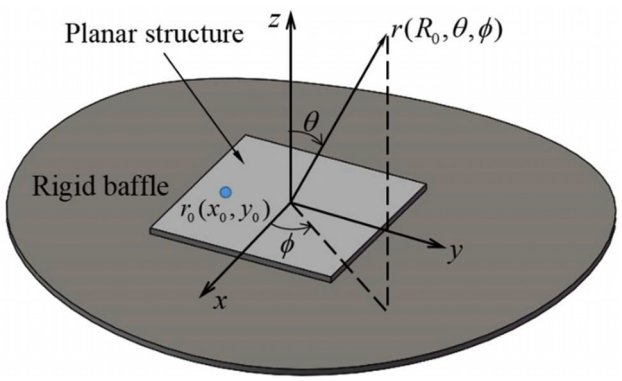

FIG. 2. (Color online) Coordinate system for the baffled plate.

where S represents the vibrating surface, ρ_a the density of air, ω the circular frequency, and k the acoustic wavenumber. r is a position vector for a receiver position in the far field, r_0 is a position vector on the vibrating surface S. $\boldsymbol{v}(r_0)$ is the complex velocity normal to the plate surface.

In the harmonic case, the averaged acoustic intensity writes

$$\vec{\boldsymbol{I}} = \frac{1}{2}\mathrm{Re}\left[\boldsymbol{p}(r)\vec{\boldsymbol{u}}^{*}(r)\right], \tag{5}$$

where $\boldsymbol{p}(r)$ and $\vec{\boldsymbol{u}}(r)$ are, respectively, the pressure and particle velocity. * denotes complex conjugate and Re the real part.

The sound power can be calculated using either far-field or near-field methods. Adopting the far-field assumption and integrating the acoustic intensity in Eq. (5) over a chosen hemispherical surface yield the total radiated sound power as

$$W = \int_0^{2\pi}\int_0^{\pi/2}\frac{|\boldsymbol{p}(R_0,\theta,\phi)|}{2\rho_a c_a}r^2\sin\theta d\theta d\phi, \tag{6}$$

where θ is the polar angle, ϕ the azimuth angle, and c_a the speed of sound.

For the near-field calculation, the vibration velocity at a point (x_0, y_0) can be expressed as

$$v(x_0,y_0) = \sum_{i=1}^{p}\sum_{j=1}^{q}\dot{a}_{ij}(t)\varphi_i(\xi)\varphi_j(\eta). \tag{7}$$

Considering the ABH-specific strong wavelength variation over the plate and the need of reaching high frequency range, Daubechies wavelet scaling functions (DWs) are used as the admissible functions to capture the local details of the vibration field. DWs are a compactly supported and orthogonal set that can be scaled to accommodate both localized and smooth variations, expressed as $\varphi_i(\xi) = 2^{m/2}\varphi(2^m\xi - i)$ and $\varphi_j(\eta) = 2^{m/2}\varphi(2^m\eta - j)$. The three parameters describing the properties are the compactly supported length (L), resolution (m), and translation (i,j). DWs are completely localized in $(0, L-1)$. To avoid singularity, the numbers of terms truncated are $p = q = 2^m + L - 2$.

Based on Eq. (7) and segmenting the plate into N cells as elementary radiators, a velocity vector $\boldsymbol{v}$ can be constructed and expressed in a matrix form as

$$\boldsymbol{v} = \boldsymbol{\Phi}\dot{\boldsymbol{A}}, \tag{8}$$

in which elements of $\boldsymbol{\Phi}$ are $\varphi_i(\xi)\varphi_j(\eta) = 2^m\varphi(2^m\xi - i)\varphi(2^m\eta - j)$ with $i,j = 1,2,\ldots,2^m + L - 2$. $\dot{\boldsymbol{A}}$ is a vector of dimension $(2^m + L - 2)\times 1$ containing the time derivatives of $a_{ij}(t)$; $\boldsymbol{\Phi}$ is a $N \times (2^m + L - 2)$ matrix. Subsequently, the radiated sound power in the near field writes

$$W = \dot{\boldsymbol{A}}^{H}(\boldsymbol{\Phi}^{H}\boldsymbol{R}\boldsymbol{\Phi})\dot{\boldsymbol{A}}, \tag{9}$$

in which the superscript H is the Hermitian transpose operator; and $\boldsymbol{R}$ the radiation resistance matrix, expressed as

$$\boldsymbol{R} = \frac{\omega^2\rho_a(\Delta S)^2}{4\pi c_a}\frac{\sin(kr_{m_0n_0})}{r_{m_0n_0}}, \tag{10}$$

where $\Delta S = S/N$ is the area of each elementary radiator on the plate and $m_0 = 1, 2, \ldots, N$, $n_0 = 1, 2, \ldots, N$.

Upon obtaining the velocity $\boldsymbol{v}$ in Eq. (8) and the sound power W in Eq. (9), the sound radiation efficiency can also be calculated as[26]

$$\sigma = \frac{W}{\rho_0 c_0 S \langle |\boldsymbol{v}|^2 \rangle}, \tag{11}$$

where $\langle |\boldsymbol{v}|^2 \rangle$ represents the spatially averaged mean square velocity over the plate of a total area S. This definition applies to the entire plate, part of the plate or one particular structural mode. In the latter case, the terminology of modal radiation efficiency will be used.

To obtain the vibration velocity in Eq. (8) and the sound power in Eq. (9), $\boldsymbol{A}$ should be calculated through Eq. (3) in which $\boldsymbol{M}$ and $\boldsymbol{K}$ involves the calculation of the 2-D connection coefficients that are the finite integrals of DWs and their derivatives. The general form of 2-D connection coefficients writes

$$I_{r,i,s,j} = \int_{\eta_1}^{\eta_2} \int_{\xi_1}^{\xi_2} [h(\xi,\eta)]^n \varphi_r^{(\alpha_\xi)}(\xi) \varphi_i^{(\beta_\xi)}(\xi) \varphi_s^{(\alpha_\eta)}(\eta) \varphi_j^{(\beta_\eta)}(\eta) d\xi d\eta, \tag{12}$$

where ξ_1 and ξ_2 are, respectively, the lower and upper limits along ξ direction; and η_1 and η_2 along η direction. n is equal to 1 or 3 and $r, s = 1, 2, \ldots, 2^m + L - 2$. $\alpha_\xi, \beta_\xi, \alpha_\eta$, and β_η are the orders of derivatives of DWs. The double integral in Eq. (12) can be calculated through 2-D Gaussian integration method which takes the following standard form

$$\int_{-1}^{1} \int_{-1}^{1} f(\xi,\eta) d\xi d\eta = \sum_{i=1}^{M_0} \sum_{j=1}^{N_0} H_i H_j f(\xi_i, \eta_j), \tag{13}$$

where H_i and H_j are the weighting coefficients, $f(\xi_i, \eta_j)$ is the value of the integrand at the Gauss point (ξ_i, η_j), and M_0, N_0 the number of Gauss points. As DWs have no closed-form solutions, DWs and their values of derivatives in Eq. (12) are obtained using a recursive procedure.[21]

2. Supersonic acoustic intensity in spatial domain

To identify the vibrating regions that effectively radiate sound into the far field. The supersonic acoustic intensity[27] will be calculated using a spatial domain approach.[23] The supersonic pressure and supersonic normal velocity are defined as[27]

$$p^{(s)}(x,y,z) = \frac{1}{4\pi^2} \int\int_{S_r} P(k_x, k_y, z) e^{-j(k_x x + k_y y)} dk_x dk_y, \tag{14}$$

$$v^{(s)}(x,y,z) = \frac{1}{4\pi^2} \int\int_{S_r} V(k_x, k_y, z) e^{-j(k_x x + k_y y)} dk_x dk_y, \tag{15}$$

in which the superscript S denotes the supersonic quantity. S_r represents the integration area, defined within a circle, comprising all values of k_x and k_y such that $k_x^2 + k_y^2 \le k^2$. Analogous to Eq. (5), the supersonic acoustic intensity is defined as

$$I^{(s)}(x,y,z) = \frac{1}{2} \mathrm{Re}\left\{ p^{(s)}(x,y,z) v^{(s)}(x,y,z)^H \right\}. \tag{16}$$

In spatial domain, the calculation of the supersonic acoustic intensity is based on a two-dimensional convolution between the acoustic field and a radiation filter mask. Compared with the wave number approach, the advantage of the direct convolution method is that it avoids a Fourier transformation in wave number domain and is relatively simple to implement. To this end, a unit circle function is defined with values transitioned from zero to one at the boundary of the circle.

The convolution theorem yields

$$p^{(s)}(x,y,z) = p(x,y,z) * h^{(s)}(x,y), \tag{17}$$

where $h^{(s)}(x,y)$ is the radiation filter mask, which can be expressed as[23]

$$h^{(s)}(x,y) = \frac{k}{2\pi\sqrt{x^2+y^2}} J_1\left(k\sqrt{x^2+y^2}\right), \tag{18}$$

where J_1 is the Bessel function of first kind. Equation (17) can then be discretized as

$$p^{(s)}(x,y,z) = \Delta S \sum_{n=1}^{N} p(x'_n, y'_n, z) \cdot h^{(s)}(x - x'_n, y - y'_n), \tag{19}$$

where ΔS is the area of each plate cell. Similar treatment also applies to the velocity terms. Subsequently, using Eq. (16) allows the calculation of the supersonic acoustic intensity.

III. MODEL IMPLEMENTATION AND NUMERICAL ANALYSES

Implementation of the simulation model requires the truncation of the decomposition series in Eq. (2). As bending waves travel towards the center of the ABH indentation, structural wavelength gradually decreases. Therefore, a sufficiently large number of decomposition terms are needed to capture the local structural details.[21] For sound radiation analyses, acoustic waves should be further considered to determine various DW parameters to be used in the computation, especially above the critical frequency where acoustic wavelength becomes smaller than their structural counterparts. A careful convergence study (similar to the procedure detailed in a previous work[21]), though not detailed here, has been carried out. A balance between the accuracy (which requires a large support length L and resolution m) and the cost effectiveness of the calculation needs to be struck. Numerical tests lead to the choice of $m = 7$ and $L = 12$, which will be used in the subsequent analysis. This results in a total of 19 044 DW terms. Compared with FEM, the errors in terms of structural natural frequencies and the sound power are typically less than 3% up to 8000 Hz.

The proposed calculation scheme is further validated against the benchmark solutions on a uniform simply supported plate. Using far-field approach, Eq. (6), the sound power is calculated with 5565 integration points uniformly distributed on a hemisphere with a radius of 10 m. Meanwhile, the radiated sound power is also calculated in the near field using Eq. (9). To obtain converged results, the plate is divided into 50 000 elementary radiators to make sure the sound field can be accurately estimated. Calculated sound power using the two different methods yields consistent estimation of the radiated sound power with analytical solutions. Furthermore, modal radiation efficiencies of the first six modes of a square plate are also calculated for comparison with the classical results obtained by Wallace.[26] Results from both calculation methods show good agreement with the reference solutions.[26] Limited by the paper length, details results are not shown here. Nevertheless, it is concluded that the extended 2-D wavelet model can accurately predict the sound radiation field. For the subsequent sound radiation analyses on ABH plates, the same calculation procedure (in terms of integration scheme and number of elementary radiators) will be followed.

A. Vibration and sound fields of ABH plates

Using the model and the far-field method described in Sec. II, the sound power radiated from ABH plate is examined. Parameters used in the calculations are tabulated in Table I, for both the ABH plate and its uniform counterpart. A unit harmonic excitation force is applied at $(0.05, 0.315)$ m.

A partial damping treatment with a constant thickness $h_d = 0.3$ mm is applied within a radius of $R_d = 86.5$ mm in the central portion of the ABH cell (shown in Fig. 1). The same damping treatment is also applied to the uniform plate for comparisons. Edges of both plates are assumed to be clamped unless otherwise specified. The space-averaged mean square velocity, with reference to $\langle |v|^2 \rangle_{ref} = 1\,\mathrm{m/s}$, and the sound power radiated by both plates are compared in Fig. 3.

The cut-on frequency[17] or the characteristic frequency[21] of the ABH plate is 500 Hz. As illustrated in Fig. 3, below 500 Hz, effects of the ABH on the plate vibration and sound power are not systematic in the sense that the inclusion of ABH indentation into the plate cannot lead to any meaningful and systematic changes in neither structural vibration nor sound radiation. In the present case, it is rather the adverse effect that one can observe. However, above 500 Hz, reductions in the vibration amplitude begin to systematically show, with vibration peaks smoothened, especially at high frequencies as shown in Fig. 3(a). Meanwhile, the ABH plate

TABLE I. Geometrical and material parameters.

Geometry		Material
$a = 0.5$ m	$x_c = 0.25$ m	$E_0 = 200$ GPa
$b = 0.45$ m	$y_c = 0.25$ m	$\mu_0 = 0.3$
$h = 4.7$ mm	$\varepsilon = 0.2$/m	$\eta_0 = 0.01$
$R_{ABH} = 0.15$ m	$\gamma = 2$	$\rho_0 = 7800\,\mathrm{kg/m^3}$
$h_0 = 0.2$ mm		

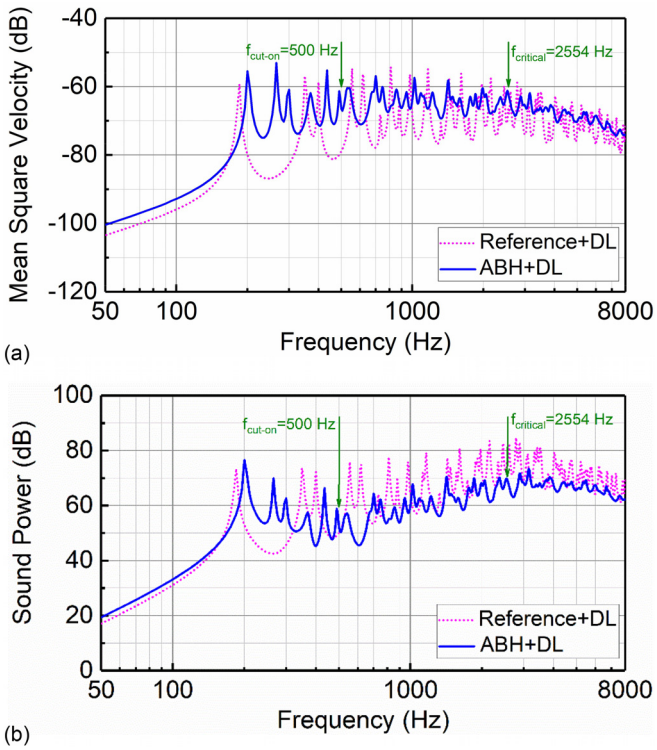

FIG. 3. (Color online) Comparisons between the reference plate and the ABH plate: (a) Space-averaged mean square velocity; (b) radiated sound power. DL denotes damping layers.

shows a significant reduction in the radiated sound power in the same frequency range. Note this is achieved by an ABH plate whose total mass is 88% that of the uniform plate due to the ABH indentation. These results demonstrate the potential and the benefit of using ABH principles to design lightweight structures. The observed sound reduction is definitely directly related to the typical ABH effect in terms of vibration energy localization and dissipation, leading to the reduced structural vibration. Meanwhile, a comparison between Figs. 3(a) and 3(b) indicates that the reduction in sound radiation seems to exceed that of the structural vibration. This points at the existence of other ABH-induced structural changes which contribute to the overall reduction of radiated sound power.

To explain this, the sound radiation efficiencies of ABH plates with/without damping layers are investigated. Again, results are compared against their uniform counterparts, as illustrated in Fig. 4. The critical frequency of the reference flat plate, $f_{critical} = (c_a^2)/2\pi\sqrt{[12\rho_0(1-\mu_0{}^2)]/E_0h^2}$, is 2554 Hz around which the radiation efficiencies peak for both plates with/without damping layers. Above this frequency, called supersonic region, the structural waves travel faster than acoustic waves, thus showing a consistently high efficiency in sound radiation, as one might expect from the basic sound radiation theory.

Figure 4 shows that the inclusion of the ABH indentation brings about significant changes in the sound radiation efficiency of the structure. (1) With or without damping, the radiation efficiencies of the ABH plates and the uniform reference plates are very similar before the first structural resonance. (2) Entering into the dynamic region and getting

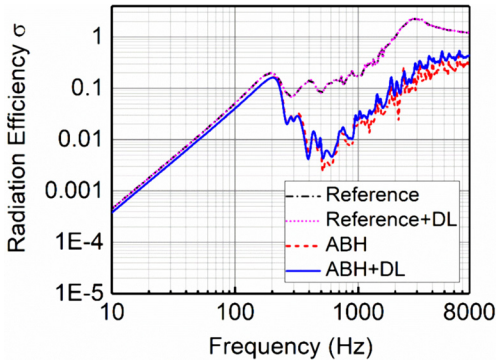

FIG. 4. (Color online) Comparisons of the sound radiation efficiencies between the reference plates and the ABH plates. DL denotes damping layers.

closer to the cut-on frequency (500 Hz), in this specific case, ABH plates show a significantly reduced radiation efficiency, compared with the uniform plates. (3) The same tendency maintains above the cut-on frequency. Above the critical frequency, the acoustically slow structural waves (also called subsonic structural waves) exist if the thinnest thickness is small enough. These waves lead to the reduced radiation efficiency, contributing to the overall reduction in the sound power of ABH plate as illustrated in Fig. 3(b). It can also be observed from Fig. 4 that the deployment of the damping layers on the flat plate does not seem to alter much the radiation efficiency due to the small amount of coating used and the energy dispersive nature of the vibration energy over the plate. However, interestingly enough, the radiation efficiency of the ABH plate with the same coating is increased above the cut-on frequency in this particular case.

To ascertain this, influences of the stiffness and the mass of the damping layer are considered separately in the ABH plate and shown in Fig. 5. As can be seen, the mass of the damping layer has a negligible effect on the radiation efficiency. On the contrary, the effect of its stiffness is apparent. Note that the values of mass density and stiffness of damping layer used are realistic ones, consistent with those used in some reference papers.[28,29] Therefore, the results call for a careful handling of damping layer in order to maximize the sound radiation reduction.

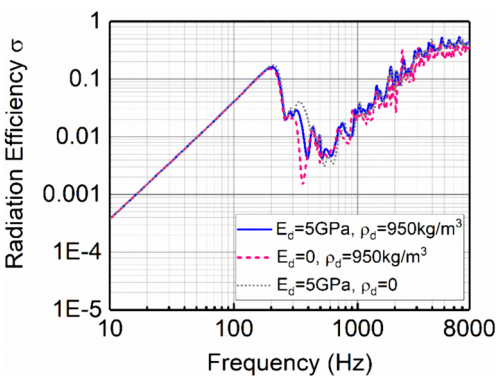

FIG. 5. (Color online) Effect of the stiffness and mass of the damping layer on the sound radiation efficiency of ABH plate.

B. Sound radiation mechanism analyses

1. Stiffness-controlled sound radiation efficiency

The observed reduction in the sound radiation efficiency below the cut-on frequency can actually be attributed to the structural stiffness changes due to the inclusion of the ABH cell. This can be demonstrated by examining a uniform plate having the same mass, but with a reduced stiffness or thickness (not shown here). Results show that the observed reduction in the sound radiation efficiency of the ABH plate before the ABH cut-on is merely due to the overall stiffness reduction of the plate, instead of the intrinsic ABH feature. This explains the aforementioned increase in the sound radiation efficiency when damping layers are used over the ABH indentation, in which case the added stiffness of the damping layers is non-negligible as compared to the thinnest part of the indentation.

2. Sound radiation within the transonic boundary

When bending waves travel across ABH boundary toward its center, with smoothly decreasing structural thickness, their phase velocity gradually reduces. For a given frequency above the critical frequency of the flat portion of the plate, a subsonic region may be created inside the ABH cell if the thickness of the ABH indentation is small enough. This subsonic region is delimited by a circle, referred to as the transonic boundary, whose radius is defined by

$$R_t = (c_a^2\sqrt{12\rho_0(1-\mu_0^2)/E_0}/(2\pi f\varepsilon))^{1/\gamma}. \tag{20}$$

As an example, the sound power radiated from the area inside the transonic boundary corresponding to 4000 Hz ($R_t = 118.4$ mm) is evaluated for three different plates: the reference flat plate and two ABH plates with/without damping layers.

Figure 6 shows that below the characteristic frequency or cut-on frequency (500 Hz), the investigated region (inside the transonic boundary) of the ABH plates (with and without damping layers) generates a higher sound power as compared with the reference plate. This is definitely due to the ABH-induced amplification of the vibration amplitude in the center area of the ABH cell, despite the aforementioned

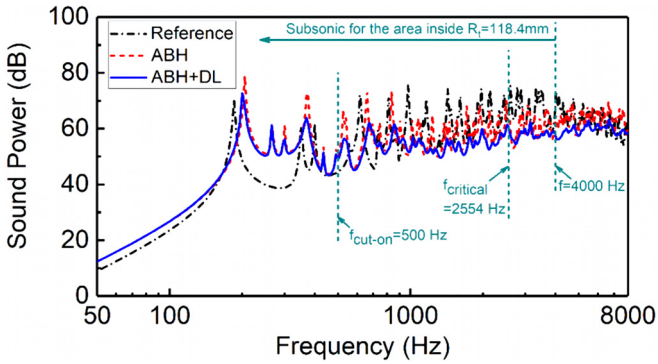

FIG. 6. (Color online) Sound power radiated from the region inside the area with a radius of 118.4 mm, corresponding to the transonic boundary at 4000 Hz.

reduction in the radiation efficiency. Above 500 Hz, the ABH effect is cut-on, resulting in an obvious sound power reduction, especially when the frequency approaches the critical frequency at $f_{critical} = 2554$ Hz. Up to 4000 Hz, the entire region inside the transonic boundary of ABH plates is subsonic. This results in the remarkably reduced sound power as compared with its counterpart in the reference panel. Above 4000 Hz, the transonic boundary starts to enter into the investigated area and keeps shrinking with the increase of the frequency, containing both subsonic and supersonic structural waves, along with greatly concentrated vibration energy. When this happens, the sound power reduction, albeit clearly observable, becomes less significant due to the existence of acoustically fast structural waves.

3. Sound radiation efficiency with transonic boundary changes

Variations of the sound radiation efficiency along with transonic boundary changes are quantified. Specifically, the radiation efficiency of a series of concentric rings, moving from the inside to the outside of the transonic boundary is investigated. In each step, the width of the rings is kept constant, $\Delta R = 1/6R_t$, as shown in Fig. 7(a). The radiation efficiencies of the rings at different frequencies (from 4000 to 8000 Hz) are compared in Fig. 7(b). At each frequency, the inner ring radius R_{inner} is normalized by its corresponding transonic boundary radius.

When $R_{inner}/R_t > 1.0$ [Fig. 7(b)], the ring moves outside the transonic boundary and enters into supersonic region; as a result, its radiation efficiency is consistently high. When the rings are inside their respective transonic boundaries, e.g., $R_{inner}/R_t < 1.0$, the sound radiation efficiency of the rings dwells at relatively low levels. While the rings passing through the transonic boundary, their corresponding radiation efficiencies undergo a sharp rise. This variation in the sound radiation efficiency is consistent with what one might expect from classical structural acoustic theory.

4. Numerical illustration of the supersonic acoustic intensity

To further illustrate the sound radiation properties of the ABH plate, various forms of acoustic intensity are calculated using the extended 2-D DW model, in comparison with its uniform counterpart for a few selected representative frequencies. The acoustic pressure over the vibrating surface and the baffle is calculated using Rayleigh integral in Eq. (4). Supersonic acoustic intensity maps are compared with the classical acoustic intensity maps. Variations of the supersonic acoustic intensity alongside the transonic boundary changes are also illustrated.

To verify the spatial domain calculation scheme detailed in Sec. II B 2, supersonic acoustic intensities for an edge mode and a corner mode of a simply supported plate were calculated. The results were shown to be consistent with those obtained by Williams[27] using wave number approach. For the sake of brevity, these results are not included here.

Figures 8(a) and 8(b) show the supersonic acoustic intensity of the uniform plate and ABH plate, respectively, at 2000 Hz which is below the critical frequency. To facilitate the comparison, the same scale is used for both plots. Supersonic acoustic intensity maps of the uniform plate in Fig. 8(a) show that effective sound radiation is basically from the two edges of the panel along y direction, which resembles the edge mode radiation, although the frequency is not a structural natural frequency to warrant perfect radiation cancellation as expected from the classical structural radiation theory. In comparison, the inclusion of the ABH indentation alters the radiation pattern as shown in Fig. 8(b). Nevertheless, effective sound radiation still originates from the edge of the panel with a more scattered pattern and a reduced level as compared to the uniform plate. Classical acoustic intensity map of the ABH plate, Fig. 8(c), shows that because of the energy concentration, the energy level inside ABH cell is indeed very high, with both positive and negative values, specific to the near-field feature of the sound radiation. With the circulating intensity being removed, supersonic acoustic intensity indeed allows for the identification of the hot spots over the plate, which are responsible for effective sound radiation into the far field. In this case, it is predominantly confined to the uniform part outside the ABH boundary, as shown in Fig. 8(b).

Following the same procedure, evolutions of these intensity maps with increasing frequencies ($f = 4200$ Hz and 7300 Hz) are illustrated from Figs. 8(d) to 8(i). Meanwhile, changes of the corresponding transonic boundary (marked by a dash circle inside the ABH boundary) are also shown

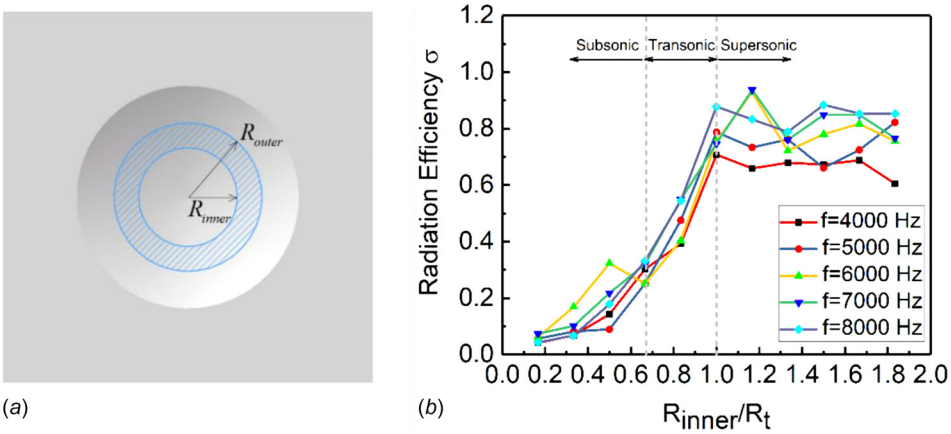

(a) (b)

FIG. 7. (Color online) Radiation of a ring moving from inside to the outside of the ABH indentation: (a) definition of the ring; (b) the radiation efficiency of the rings.

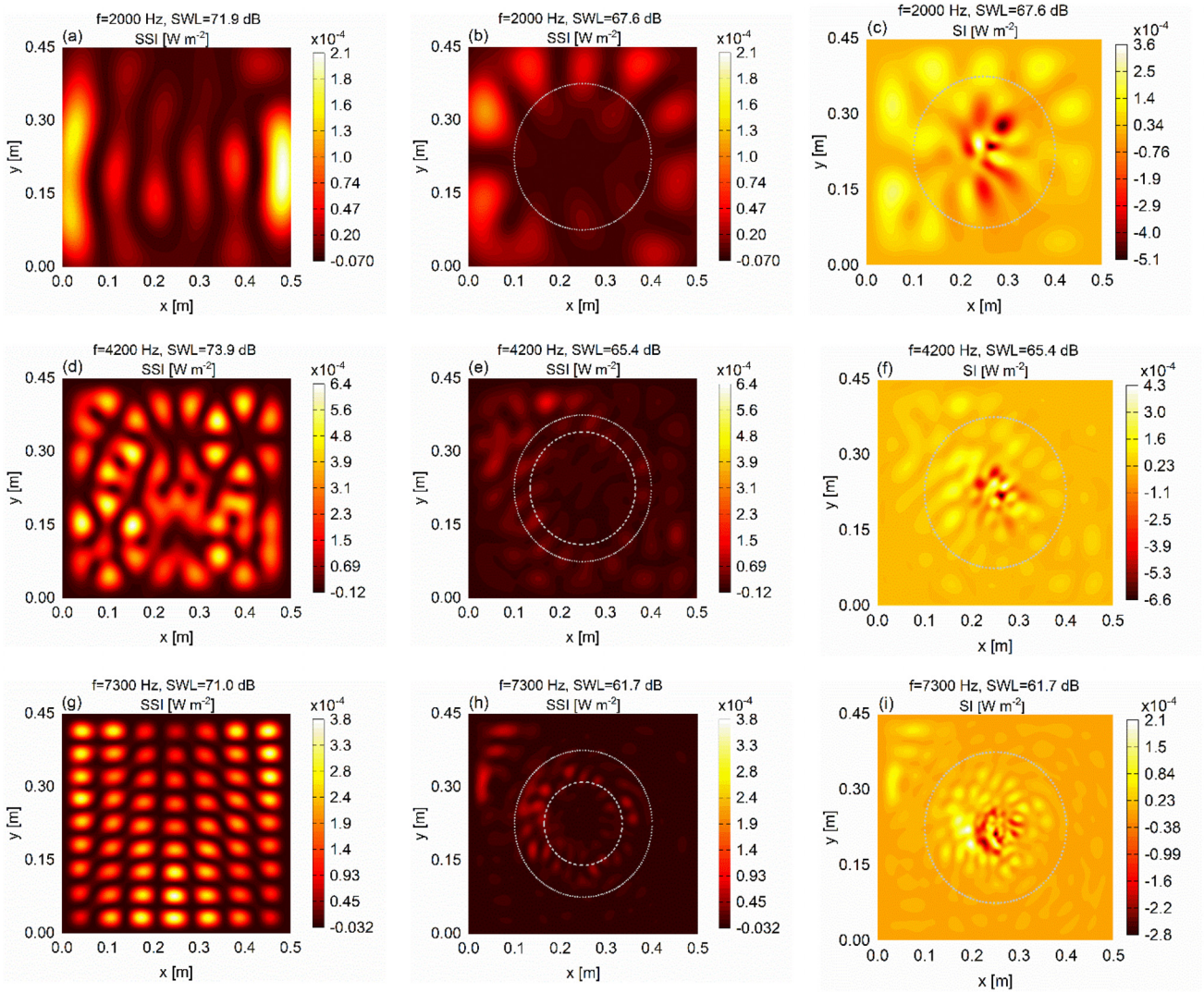

FIG. 8. (Color online) Acoustic intensity maps: (a),(b),(c) f = 2000 Hz; (d),(e),(f) f = 4200 Hz; (g),(h),(i) f = 7300 Hz. (a),(d),(g) Supersonic acoustic intensity of the reference plate; (b),(e),(h) supersonic acoustic intensity of the ABH plate; (c),(f),(i) acoustic intensity of the ABH plate. The dot circle denotes the ABH periphery and the dash circle the transonic boundary. SSI indicates the supersonic acoustic intensity; SI the acoustic intensity and SWL the total radiated sound power.

for the three arbitrarily chosen frequencies, all above the critical frequency of the flat panel. For the flat plates [Figs. 8(d) and 8(g)], when the frequency increases, the sound radiation pattern shown by the supersonic intensity maps become more regular over the entire plate surface, similar to the surface radiation pattern. For the corresponding ABH plate, a transonic boundary appears and gradually reduces in size with the frequency. However, different from the uniform plate, the distribution of the effective sound radiation areas becomes less regular. More specifically, apart from the upper-left corner of the panel where the excitation force is applied, most energetic sound radiators gradually move into the ring between the ABH periphery and transonic boundaries when frequency increases [Figs. 8(e) and 8(h)]. This ring area, being supersonic, exhibits high radiation efficiency and contains a considerable amount of vibration energy at the same time. In terms of intensity level, judged by the darkness of the maps (or by the colors online), it is also obvious that the flat plates radiate much more efficiently than the ABH plate does, even though the near-field acoustic intensity could be high [Figs. 8(f) and 8(i)] inside the subsonic region of the ABH plate. These results agree with the sound radiation properties along with transonic boundary changes analyzed in Sec. III B 2.

IV. CONCLUSIONS

As an alternative to conventional FEM, a 2-D DW model is established to explore the sound radiation mechanisms of a plate embedded with a circular ABH indentation. The accuracy and the efficacy of the model in predicting various acoustic parameters are demonstrated and validated. The model allows the exploration of ABH-specific sound radiation features in relation to the transonic boundary changes. Supersonic acoustic intensity in spatial domain is used to visualize the sound radiation pattern and identify the dominant sound radiation areas on the vibrating surface of the ABH plate. Numerical analyses lead to the following main conclusions:

(1) The investigated ABH plate is shown to exhibit a significantly reduced sound radiation efficiency in a broad dynamic frequency range as compared to its uniform counterpart. Physical mechanisms in different frequency ranges are revealed. Before the cut-on of the ABH effect, this is mainly due to the weakening of the overall structural stiffness, which persists until the critical frequency. Above the critical frequency, the subsonic region within the transonic boundary results in an impaired sound radiation efficiency of the plate due to the subsonic structural waves. Supersonic acoustic intensity maps show that the regularly distributed supersonic waves over the flat plate are altered by the presence of the ABH indentation. As a result, the far-field acoustic energy is mainly generated by the ring area between the ABH periphery and the corresponding transonic boundary.

(2) For the investigated configuration, an increase in the sound radiation efficiency of the ABH panel is observed, which is caused by the added stiffness effect of the damping layer. This points at the need of striking a balance between the dual effects of the damping layers: damping enhancement and stiffness-induced increase in the sound radiation efficiency of the structure.

ACKNOWLEDGMENTS

The authors thank the Research Grant Council of the Hong Kong SAR (PolyU 152017/17E) and the National Science Foundation of China (No. 11532006) for their support.

[1]F. J. Fahy and P. Gardonio, *Sound and Structural Vibration: Radiation, Transmission and Response* (Academic, Burlington, MA, 2007).
[2]D. J. Mead, *Passive Vibration Control* (Wiley, New York, 1999).
[3]M. Mironov, "Propagation of a flexural wave in a plate whose thickness decreases smoothly to zero in a finite interval," Sov. Phys. Acoust. **34**, 318–319 (1988).
[4]V. Krylov and F. Tilman, "Acoustic 'black holes' for flexural waves as effective vibration dampers," J. Sound Vib. **274**, 605–619 (2004).
[5]V. V. Krylov and R. Winward, "Experimental investigation of the acoustic black hole effect for flexural waves in tapered plates," J. Sound Vib. **300**, 43–49 (2007).
[6]V. Denis, F. Gautier, A. Pelat, and J. Poittevin, "Measurement and modelling of the reflection coefficient of an Acoustic Black Hole termination," J. Sound Vib. **349**, 67–79 (2015).
[7]L. Tang, L. Cheng, H. Ji, and J. Qiu, "Characterization of acoustic black hole effect using a one-dimensional fully-coupled and wavelet-decomposed semi-analytical model," J. Sound Vib. **374**, 172–184 (2016).
[8]T. Zhou, L. Tang, H. Ji, J. Qiu, and L. Cheng, "Dynamic and static properties of double-layered compound acoustic black hole structures," Int. J. Appl. Mech. **9**, 1750074 (2017).
[9]O. Aklouche, A. Pelat, S. Maugeais, and F. Gautier, "Scattering of flexural waves by a pit of quadratic profile inserted in an infinite thin plate," J. Sound Vib. **375**, 38–52 (2016).
[10]D. O'Boy, V. V. Krylov, and V. Kralovic, "Damping of flexural vibrations in rectangular plates using the acoustic black hole effect," J. Sound Vib. **329**, 4672–4688 (2010).
[11]V. Georgiev, J. Cuenca, F. Gautier, L. Simon, and V. Krylov, "Damping of structural vibrations in beams and elliptical plates using the acoustic black hole effect," J. Sound Vib. **330**, 2497–2508 (2011).
[12]P. A. Feurtado and S. C. Conlon, "An experimental investigation of acoustic black hole dynamics at low, mid, and high frequencies," J. Vib. Acoust. **138**, 061002 (2016).
[13]E. Bowyer, D. O'Boy, V. V. Krylov, and J. L. Horner, "Effect of geometrical and material imperfections on damping flexural vibrations in plates with attached wedges of power law profile," Appl. Acoust. **73**, 514–523 (2012).
[14]W. Huang, H. Ji, J. Qiu, and L. Cheng, "Analysis of ray trajectories of flexural waves propagating over generalized acoustic black hole indentations," J. Sound Vib. **417**, 216–226 (2018).
[15]L. Zhao, "Passive vibration control based on embedded acoustic black holes," J. Vib. Acoust. **138**, 041002 (2016).
[16]L. Zhao, S. C. Conlon, and F. Semperlotti, "Broadband energy harvesting using acoustic black hole structural tailoring," Smart Mater. Struct. **23**, 065021 (2014).
[17]S. C. Conlon, J. B. Fahnline, and F. Semperlotti, "Numerical analysis of the vibroacoustic properties of plates with embedded grids of acoustic black holes," J. Acoust. Soc. Am. **137**, 447–457 (2015).
[18]P. A. Feurtado and S. C. Conlon, "Wavenumber transform analysis for acoustic black hole design," J. Acoust. Soc. Am. **140**, 718–727 (2016).
[19]E. Bowyer and V. V. Krylov, "Experimental study of sound radiation by plates containing circular indentations of power-law profile," Appl. Acoust. **88**, 30–37 (2015).
[20]P. A. Feurtado and S. C. Conlon, "Transmission loss of plates with embedded acoustic black holes," J. Acoust. Soc. Am. **142**, 1390–1398 (2017).
[21]L. Ma, S. Zhang, and L. Cheng, "A 2D Daubechies wavelet model on the vibration of rectangular plates containing strip indentations with a parabolic thickness profile," J. Sound Vib. **429**, 130–146 (2018).
[22]E. G. Williams, *Fourier Acoustics: Sound Radiation and Nearfield Acoustical Holography* (Academic, San Diego, 1999).
[23]E. Fernandez-Grande, F. Jacobsen, and Q. Leclere, "Direct formulation of the supersonic acoustic intensity in space domain," J. Acoust. Soc. Am. **131**, 186–193 (2012).
[24]L. Cheng and R. Lapointe, "Vibration attenuation of panel structures by optimally shaped viscoelastic coating with added weight considerations," Thin Wall. Struct. **21**, 307–326 (1995).
[25]R. L. Clark, W. R. Saunders, and G. P. Gibbs, *Adaptive Structures: Dynamics and Control* (Wiley, New York, 1998).
[26]C. Wallace, "Radiation resistance of a rectangular panel," J. Acoust. Soc. Am. **51**, 946–952 (1972).
[27]E. G. Williams, "Supersonic acoustic intensity on planar sources," J. Acoust. Soc. Am. **104**, 2845–2850 (1998).
[28]V. Denis, A. Pelat, F. Gautier, and B. Elie, "Modal overlap factor of a beam with an acoustic black hole termination," J. Sound Vib. **333**, 2475–2488 (2014).
[29]S.-Y. Kim and D. Lee, "Numerical analysis of wave energy dissipation by damping treatments in a plate with acoustic black holes," J. Mech. Sci. Technol. **32**, 3547–3555 (2018).